Design scheme of new multifunctional Heusler compounds for spin-transfer torque applications

J. Winterlik[1], S. Chadov[1], V. Alijani[1], T. Gasi[1], K. Filsinger[1], B. Balke[1], G. H. Fecher[1], C.A. Jenkins[1,2], J. Kübler[3], G. D. Liu[4], L. Gao[5], S. S. P. Parkin[5] & C. Felser[1*]

[1]*Institute of Inorganic and Analytical Chemistry, Johannes Gutenberg - University, 55099 Mainz, Germany*

[2]*Advanced Light Source, Lawrence Berkeley National Laboratory, Berkeley, CA, 94720, USA*

[3]*Institute of Solid State Physics, Technische Universität, 64289 Darmstadt, Germany*

[4]*School of Material Sciences and Engineering, Hebei University of Technology, Tianjin 300130, China*

[5]*IBM Research Division, Almaden Research Center, San Jose, CA 95120, USA*

To whom correspondence should be addressed; E-mail: felser@uni-mainz.de

Heusler compounds represent a remarkable class of materials with more than 1,500 members and a wide range of extraordinary multifunctionalities including half-metallic high-temperature ferri- and ferromagnets[1], multiferroic shape memory alloys[2-4] and topological insulators[5-7] highly attractive for spintronics[8], energy technologies[9] and magnetocaloric applications[10]. Recent development of efficient spintronic devices is focused on exploiting the spin-transfer torque (STT)[11-13] phenomenon. The key property for the corresponding materials is a strong magnetocrystalline anisotropy (MCA) energy providing the out-of-plane magnetization, the so-called perpendicular magnetocrystalline anisotropy (PMA). In this letter we introduce the family of tetragonal Heusler compounds as optimal materials for spin transfer torque magnetic random access memory (STT-MRAM) data storage and for spin torque oscillators (STO) in telecommunication. With moderate saturation magnetizations (M_S) of 0.2 – 4.0 μ_B, high Curie temperatures (T_C) of up to 800 K, high spin polarizations and the lattice constants well-matching with MgO, they fulfil all the required properties. We also present a scheme for their systematic design based on tuning their chemical composition in order to shift the van Hove band structure singularity in the proximity of the Fermi energy (E_F).

Nowadays spintronics substantially focuses on exploiting the STT effect since the improvement of data storage permanently requires to minimize the distance between storage elements. The major advantage of the spin-injection compared to the field-induced switching of the magnetization direction is that the stray fields causing the undesired writing on vicinal elements do not appear. New and ideally rare-earth-free materials for implementation in STT-MRAM and STO devices require high spin polarizations and T_C but low M_S and Gilbert damping in order to facilitate the sufficiently low switching currents according to the Slonczewski-Berger equation[11,12]. For an efficient and thermally stable switching, a PMA material would furthermore be preferable.

Many Heusler compounds exhibit high spin polarization and high T_C[14,15], which are important for the stable performance of spintronic devices at room temperature and above. Heusler compounds with a cubic-to-tetragonal martensitic transition are well-known in the context of magnetic shape memory alloys[16,17]. One of the most recent realizations was the uncovering of their attractivity for STT applications[18]. Combined experimental and theoretical studies of the bulk properties by Winterlik *et al.*[19] suggested one of them, Mn_3Ga, to exhibit a strong PMA, which was later realized in a thin film by Miyazaki's group[20]. The proposed high spin polarization was confirmed by Coey *et al.*[21] Recently an exceptionally low Gilbert damping and long-lived ultrafast spin precession of up to 280 GHz in $Mn_{3-x}Ga$ was demonstrated by Mizukami *et al.*[22].

A tunable PMA material for the STT-MRAMs is supposed to contain a fixed layer with strong MCA and an easily switchable free layer. The drawback of Mn_3Ga is the lattice mismatch with MgO (the most commonly used tunneling barrier) which leads to

an unsatisfactory tunnel magnetoresistance (TMR) in devices. However, the presented design scheme opens a straightforward access to a large number of PMA-Heusler compounds, which fulfill all needs: tunability of the magnetic moment and the lattice parameters, high spin polarization, high T_C, high MCA due to a tetragonal distortion of the unit cell, and low Gilbert damping due to moderate spin-orbit coupling (SOC) of the *3d* and *4p* elements in Heusler compounds compared to many other anisotropic magnetic compounds such as FePt.

In the following we illustrate a scheme for the systematic design of new Mn_2YZ Heusler compounds and the corresponding experimental results, which confirm its functionality. The underlying idea as shown in Figure 1 is that the structural instability of the cubic phase is typically indicated by the so-called van Hove singularities[23] in proximity of E_F resulting in high peaks of the density of states (DOS). These singularities can be straightforwardly identified by *ab-initio* band structure calculations (for more details, see the Supplementary information). If all reasonable electronic relaxation mechanisms including magnetism cannot remove the singularity, the only way to escape from this type of instability is by undergoing a structural distortion, thereby reducing the DOS at E_F. This necessary condition for the tetragonal strain is identical to the molecular Jahn-Teller-Effect[24]. In Heusler compounds the octahedrally coordinated Mn atoms typically exhibit the d^4-configuration of Mn^{3+} ions and are thus very susceptible to Jahn-Teller distortions (the characteristics of the crystal field splitting on the Mn atoms are shown in Supplementary Figure 2). If the corresponding degenerated e_g states are found at E_F for $c/a = 1$, then a local minimum of the total energy will be shifted towards $c/a \neq 1$ (the typical value of tetragonal Heusler compounds is close to 1.3, however the whole range varies within $0.95 < c/a < 1.43$).

What remains is to evaluate the relative stability of the material for different distortions. The derived energy profiles allow to distinguish between a stable tetragonal distortion (Mn_3Ga), a stable cubic structure (Mn_2CoGa), and a shape memory system (Mn_2NiGa) (the corresponding results of the first-principal calculations are shown in Supplementary Figure 1). Typical profiles of stable cubic compounds exhibit the total energy minimum at $c/a = 1$, those of tetragonal compounds at $c/a \neq 1$. Shape memory compounds exhibit two distinct minima (cubic and tetragonal structures) separated by a small energy barrier. $Mn_{2.5}Co_{0.5}Ga$ is a system, which appears exactly at the borderline between the stable and unstable cubic structures.

The whole manifold of possible structures formed by Mn_2YZ Heusler compounds is shown in Figure 2. When the Y element is more electronegative than the Mn atom, the so-called “inverse Heusler structure” including three different magnetic sublattices is formed. Figure 3 shows the calculated MCA of tetragonal compounds and their experimental realization. Obviously, the MCA of the Mn_2-based compounds follow simple trends. First, it strongly depends on the number of valence electrons (N_V), which is directly related to ΔE, the distance from the van Hove singularity to E_F; second, they scale up with the SOC by going from Y = *3d* (Ni) via *4d* (Rh) to *5d* (Ir). The highest MCA was found for Mn_2PtSn (3.04 meV) but its low T_C (374 K) constitutes a drawback. Mn_3Ga with a calculated MCA of about 1 meV, which is in excellent agreement with the experimental observation[19], can already compete with the typical material used for the STT compound FePt (MCA is close to 3 meV[25]). As the coercive fields of both materials are very similar, the difference in MCA is only due to the lower magnetic moment of Mn_3Ga, which is on the other hand necessary to ensure a sufficiently low switching current. Mn_3Ga also exhibits a substantially lower Gilbert

damping (one order of magnitude) and much higher TMR. It is important to emphasize that the tetragonal distortion does not automatically guarantee the perpendicular alignment of magnetization as determined for the related tetragonal Heusler compounds Rh_2YZ[26] since the MCA oscillates as a function of *c/a*. But this can be verified by calculations.

Figure 3 **b** gives an overview of the new cubic and tetragonal Mn_2YZ Heusler compounds, which were identified with the proposed design scheme, synthesized, and characterized with respect to crystal structures and magnetism. Most of these materials are yet unreported and were characterized experimentally for the first time by following the structure-to-property-relations of Mn_2YZ. The current literature reports only Mn_3Ga, Mn_2CoSn, Mn_2NiGa, Mn_2NiSn, and Mn_2RuGa[19,27-29]. Two trends are obvious: Mn_2YGa compounds with the exception of Y = Co tend to form tetragonal structures with *3d* elements at the Y position. In contrast, the *4d* and *5d* elements form only cubic Mn_2YGa. The opposite situation takes place in the Mn_2YSn series, which contains several tetragonal compounds with *4d* and *5d* elements, while only cubic (and hexagonal, not mentioned here) phases are found with *3d* elements. Consequently, the lowest MCA were obtained in the known shape memory systems Mn_2NiGa and Fe_2MnGa. The tetragonal compounds with *3d* elements in the Y position exhibit high MCA and high T_C of 500 K and above. The tetragonal compounds with *4d* and *5d* elements in the Y position exhibit high MCA but low coercivities, which is also related to their low T_C.

Starting with the stoichiometric Mn_3Ga compound we can explore the whole phase diagram of $Mn_{3-x}Y_xZ$. Exemplarily we consider the detailed experimental

characterizations of the three systems $Mn_{3-x}Fe_xGa$, $Mn_{3-x}Co_xGa$, and $Mn_{3-x}Ni_xGa$ as shown in Figure 3. The entire series of alloys investigated exhibits high T_C. The $Mn_{3-x}Co_xGa$ system exhibits an interesting feature: while the tetragonal Mn-rich alloys are hard-magnetic and similar to $Mn_{3-x}Ga$, the cubic Co-rich alloys exhibit soft-magnetic hysteresis loops and follow the Slater-Pauling rule perfectly. These characteristics facilitate the MCA tunability by simply varying the Co concentration. While the tetragonal alloys exhibit the features typically attractive for STT applications (high T_C, strong PMA, high spin polarization, low M_S), the cubic systems represent the second big class of 100% spin polarized half-metallic Heusler materials robustly following the Slater-Pauling rule as in case of the Co_2YZ compounds. The tetragonal $Mn_{3-x}Co_xGa$ alloys are still highly spin-polarized due to a pseudo-gap in one spin channel. Tuning between the spin polarization on one hand, but on the other hand between high and low degrees of magnetic anisotropy offers the opportunity of tailoring the magnetic properties continuously as desired. The magnetic couplings in $Mn_{3-x}Co_xGa$ correspond to the arrangements shown in Figure 1 **b**, **d**. Co atoms are always tetrahedrally coordinated while Mn atoms are found in both tetrahedral and octahedral environments. Being next neighbors, they carry opposing spins.

The ferrimagnetic Mn-rich alloys $Mn_{3-x}Fe_xGa$ are similar to $Mn_{3-x}Ga$[19] but exhibit smaller coercivity and magnetic remanence. These alloys can be used as free-layer materials, which must not be too hard to allow for easy switching. The phases $Mn_{2.5}Fe_{0.5}Ga$ – Mn_2FeGa despite their tetragonal structures exhibit magnetic moments in agreement with the Slater-Pauling rule. An exceptional structure is found for Mn_2FeGa, which on a first glance appears to be completely disordered face-centered cubic (A1). The Rietveld analysis of the diffraction pattern, however, confirms the

inverse tetragonally distorted Heusler structure with a *c/a* ratio close to the square root of 2. Reducing the Fe amount only by 10% is already sufficient to uncover the tetragonal splits of certain reflections. The Fe-rich phases show strong magnetic moments on Mn culminating in a magnetic moment of nearly 4 μ_B in Fe_2MnGa. The latter occurs due to decreasing contributions of the antiparallely aligned Fe spins. We have ascertained by Moessbauer spectroscopy that the Fe atoms carry only small magnetic moments (details are shown in the Supplementary information). The magnetic moment is almost completely carried by localized octahedral Mn atoms very similar to d^4 Mn^{3+} ions. While Fe_2MnGa is a shape memory compound, the Mn-rich alloys are interesting for the STT applications.

The alloys $Mn_{3-x}Ni_xGa$ show an exceptional variety of anisotropies and shapes of magnetic hysteresis loops. Mn-doping of the known shape memory compound Mn_2NiGa, which is relatively soft-magnetic, leads first to a strong decrease of the magnetic moment (0.20 μ_B for $Mn_{2.4}Ni_{0.6}Ga$) but then, similar to $Mn_{3-x}Co_xGa$, it increases up to the value of Mn_3Ga. (Detailed information about the magnetic characteristics of the important tetragonal Heusler compositions is given in Supplementary Table 1). Generally, in all presented alloy series the magnetic moments decrease with decreasing Mn content, pass through a minimum, and then increase again. A similar trend is observed in the corresponding T_C dependencies. For the different Y atoms all minima are found in the range within $24.8 < N_V < 25.8$ electrons per formula unit. This very interesting feature is strongly related with the similarity of electronic structures of the alloys.

Such a “virtual-lab” approach combining the indications from the first-principles calculations and the subsequent experimental realization opens an enormous phase space of tetragonal Mn_2YZ Heusler compounds with tunable PMA, which allow for the fabrication of universally applicable spintronic devices, combining many advantages and avoiding many disadvantages of state of the art. With respect to magnetic tunnel junctions, Mn_2-based Heusler compounds inherently offer all the prerequisites, which are currently simulated by the complex synthetic ferrimagnets consisting of three layers. Two of those can be economized when substituted by a highly spin-polarized Heusler ferrimagnet. Low magnetic moments, low Gilbert damping, and high spin polarizations ensure the low switching currents. High T_C allows for high-temperature performance whereas the high PMA guarantees the nonvolatility of memories. According to our design scheme $Mn_{2.7}Co_{0.3}Ga$ is an ideal material for STT applications. It exhibits strong MCA, high T_C (750 K), and an even lower magnetic moment (0.58 μ_B) compared to Mn_3Ga. Another tetragonal Heusler compound, Mn_2FeGa, is highly efficient as a free layer material due to its small magnetic moment and coercivity. Similar to Mn_3Ga, the lattice mismatch with MgO constitutes a certain drawback, However, this is typically improved by doping with small amounts of Sn, which leads to an increase of the lattice parameter.

References

1. Felser, C., Fecher, G. H. & Balke, B. Spintronics: A Challenge for Materials and Solid-State Chemistry. *Angew. Chem. Int. Ed.* **46,** 668-699 (2007).

2. Kainuma, R. *et al.* Magnetic-field-induced shape recovery by reverse phase transformation. *Nature* **439,** 957-960 (2006).

3. Krenke, T. *et al.* Inverse magnetocaloric effect in ferromagnetic Ni-Mn-Sn alloys. *Nature Mater.* **4,** 450-454 (2005).

4. Takeuchi, I. *et al.* Identification of novel compositions of ferromagnetic shape-memory alloys using composition spreads. *Nature Mater.* **2,** 180-184 (2003).

5. Chadov, S. *et al.* Tunable multifunctional topological insulators in ternary Heusler compounds. *Nature Mater.* **9,** 541-545 (2010).

6. Lin, H. *et al.* Half-Heusler ternary compounds as new multifunctional experimental platforms for topological quantum phenomena. *Nature Mater.* **9,** 546-549 (2010).

7. Franz, M. Topological insulators: Starting a new family. *Nature Mater.* **9,** 536-537 (2010).

8. Sakuraba, Y. *et al.* Mechanism of large magnetoresistance in Co_2MnSi/Ag/Co_2MnSi devices with current perpendicular to plane. *Phys. Rev. B* **82,** 094444 (2010).

9. Sakurada, S. & Shutoh, N. Effect of Ti substitution on the thermoelectric properties of (Zr,Hf)NiSn half-Heusler alloys. *Appl. Phys. Lett.* **86,** 082105 (2005).

10. Mañosa, L. *et al.* Giant solid-state barocaloric effect in the Ni-Mn-In magnetic shape-memory alloy. *Nature Mater.* **9,** 478-481 (2010).

11. Slonczewski, J. Current-driven excitation of magnetic multilayers. *J. Magn. Magn. Mater.* **159,** L1-L7 (1996).

12. Berger, L. Emission of spin waves by a magnetic multilayer traversed by a current. *Phys. Rev. B* **54,** 9353-9358 (1996).

13. Ikeda, S. *et al.* A perpendicular-anisotropy CoFeB-MgO magnetic tunnel junction. *Nature Mater.* 9, 721-724 (2010).

14. Wurmehl, S. *et al.* Investigation of Co_2FeSi: the Heusler compound with highest Curie temperature and magnetic moment. *Appl. Phys. Lett.* **88,** 032503 (2006).

15. Graf, T., Felser, C. & Parkin, S. S. P. Simple rules for the understanding of Heusler compounds. *Prog. Solid State Chem.* doi:10.1016/j.progsolidstchem.2011.02.001 (2011).

16. Entel, P. *et al.* Modelling the phase diagram of magnetic shape memory Heusler alloys. *J. Phys. D: Appl. Phys.* **39,** 865-889 (2006).

17. Jakob, G. & Elmers, H. J. Epitaxial films of the magnetic shape memory material Ni_2MnGa. *J. Magn. Magn. Mater.* **310,** 2779-2781 (2007).

18. Balke, B., Fecher, G: H., Winterlik, J. & Felser, C. Mn_3Ga, a compensated ferrimagnet with high Curie temperature and low magnetic moment for spin torque transfer applications. *Appl. Phys. Lett.* **90,** 152504 (2007).

19. Winterlik, J. *et al.* Structural, electronic, and magnetic properties of tetragonal $Mn_{3-x}Ga$: Experiments and first-principles calculations. *Phys. Rev. B* **77,** 0544006 (2008).

20. Wu, F. *et al.* Epitaxial $Mn_{2.5}Ga$ thin films with giant perpendicular magnetic anisotropy for spintronic devices. *Appl. Phys. Lett.* **94,** 122503 (2009).

21. Kurt, H., Rode, K., Venkatesan, M., Stamenov, P. & Coey, J. M. D. High spin polarization in epitaxial films of ferromagnetic Mn_3Ga. *Phys. Rev. B* **83,** 020405 (2011).

22. Mizukami, S. *et al.* Long-Lived Ultrafast Spin Precession in Manganese Alloys Films with a Large Perpendicular Magnetic Anisotropy. *Phys. Rev. Lett.* **106,** 117201 (2011).

23. Van Hove, L. The Occurrence of Singularities in the Elastic Frequency Distribution of a Crystal. *Phys. Rev.* **89,** 1189-1193 (1953).

24. Jahn, H. A. & Teller, E. Stability of polyatomic molecules in degenerate electronic states. I. Orbital degeneracy. *Proc. Roy. Soc. A* **161,** 220-235 (1937).

25. Lyubina, J. *et al.* Magnetocrystalline anisotropy in $L1_0$ FePt and exchange coupling in FePt/Fe_3Pt nanocomposites. *J. Phys.: Cond. Mat.* **17,** 4157–4170 (2005).

26. Gao, L. *et al.* Thin film growth and characterization of full Heusler alloys $Rh_{2-x}Co_xFeSn$ and RhCoMnSn. *Bull. Am. Phys. Soc.* **56,** T19 (2011).

27. Lakshmi, N., Pandey, A. & Venugopalan, K. Hyperfine field distributions in disordered Mn_2CoSn and Mn_2NiSn Heusler alloys. *Bull. Mater. Sci.* **25,** 309-313 (2002).

28. Brown, P. J. *et al.* Atomic and magnetic order in the shape memory alloy Mn_2NiGa. *J. Phys.: Condens. Matter* **22,** 506001 (2010).

29. Hori, T., Akimitsu, M., Miki, H., Ohoyoama, K. & Yamaguchi, Y. Magnetic properties of $(Mn_{1-x}Ru_x)_3Ga$ alloys. *Appl. Phys. A* **74,** 737-739 (2002).

Acknowledgements

This work was funded by the *Deutsche Forschungs Gemeinschaft DfG* (projects TP 1.2-A and TP 1.3-A of Research Unit *ASPIMATT* FOR 1464) and DfG-JST (FE633/6-1). Work at the ALS was supported by the U.S. Department of Energy under Contract No. DE-AC02-05CH1123. The authors are grateful for the fruitful discussions with W. Pickett and H.-J. Elmers. Vadmim Ksenofontov is acknowledged for support with Moessbauer spectroscopy.

Author contributions

All authors have contributed equally to the manuscript.

Additional information

The authors declare no competing financial interests.

Figure 1: The design scheme of tetragonal Mn_2-based Heusler compounds. a, The schematic band structure of hypothetic cubic Mn_3Ga, which represents the typical DOS of nearly all Heusler compounds exhibiting the tetragonal distortion caused by the van Hove singularity in proximity of the Fermi energy. **b**, The corresponding energy levels scheme of a Mn_2YZ Heusler compound conforms to the molecular e_g orbitals (MO) of Mn^{3+} ions with d^4-configuration as determined by present calculations. The tetragonal distortion lifts the degeneracy of the e_g orbitals. **c**, Exemplary spin-resolved densities of states of half-metallic $Mn_{2.5}Co_{0.5}Ga$ and the shape memory alloy Mn_2NiGa. In case of $Mn_{2.5}Co_{0.5}Ga$ the system is unstable in the cubic phase. This is clearly indicated by a sharp peak of DOS at E_F in one spin channel. In the DOS of Mn_2NiGa, the energy distance ΔE between the van Hove singularity and E_F is larger (→ substantially reduced DOS at E_F) resulting in a stable cubic structure.

d, The structural stability is typically analyzed by calculating the total energy as a function of the *c/a* ratio.

Figure 2: Crystal structures of different types of Mn_2YZ Heusler compounds. a, The preferred structure chosen by a composition of arbitrary transition metals Y depends on their position in the periodic system and the electronic structure of the compound (→ van Hove singularity). **b**,**c**, Different views of an inverse cubic Heusler cell. **d**, Tetragonal inverse Heusler cell with three magnetic sublattices (red, blue, and orange spheres).

Figure 3: MCA predicted for several tetragonal Heusler compounds and the experimental verification. a, Calculated MCA values. The MCA of compounds with *3d* Y elements increases upon decrease of ΔE (→ coincidence with van Hove singularity and E_F). MCA scales up with increasing SOC as well, but at the expense of higher Gilbert damping. **b**, Overview of the synthesized "stoichiometric Mn_2YZ Heusler compounds" with Z = Al, Ga, and Sn. The structures were determined using x-ray powder diffraction and Rietveld analyses.

Figure 4: Magnetic properties of $Mn_{3-x}Y_xZ$ alloys, where Y = Fe, Co, and Ni. a, **c**, **e**, The experimentally determined saturation magnetic moments at T = 5 K compared to the Slater-Pauling values. Tetragonal and cubic compounds are represented by circles and squares, respectively. Heights and widths of the inserted hysteresis loops correspond to the factual ratios. The colored arrows

represent the calculated local magnetic moments placed directly above the corresponding compositions. **b**, **d**, **f**, The T_C of the alloys.

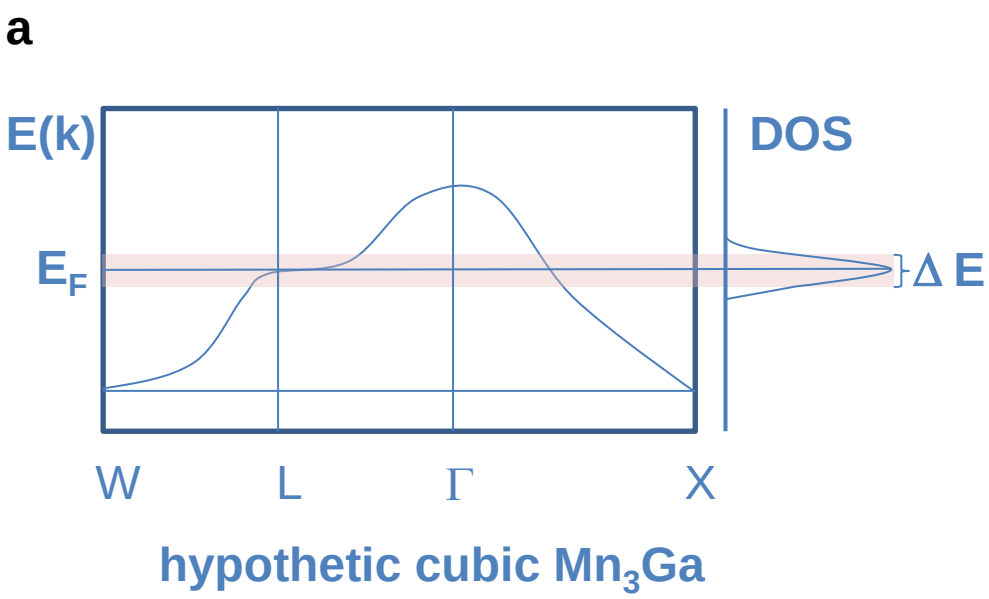
a
E(k)
DOS
E_F
Δ E
W
L
Γ
X
hypothetic cubic Mn3Ga
b
E_F
Δ E
d_x2-y2
d_z2
d_x2-y2
Mn3+
d_z2
d_xy
d_xz
d_yz
d_xy
d_xz
d_yz
cubic
tetragonal
c
DOS
DOS
E_F
Mn2.5Co0.5Ga
Mn2NiGa
d
E
Cubic
Shape memory
Tetragonal
1
≈ 1.3
c/a
Structural stability of Mn2YGa

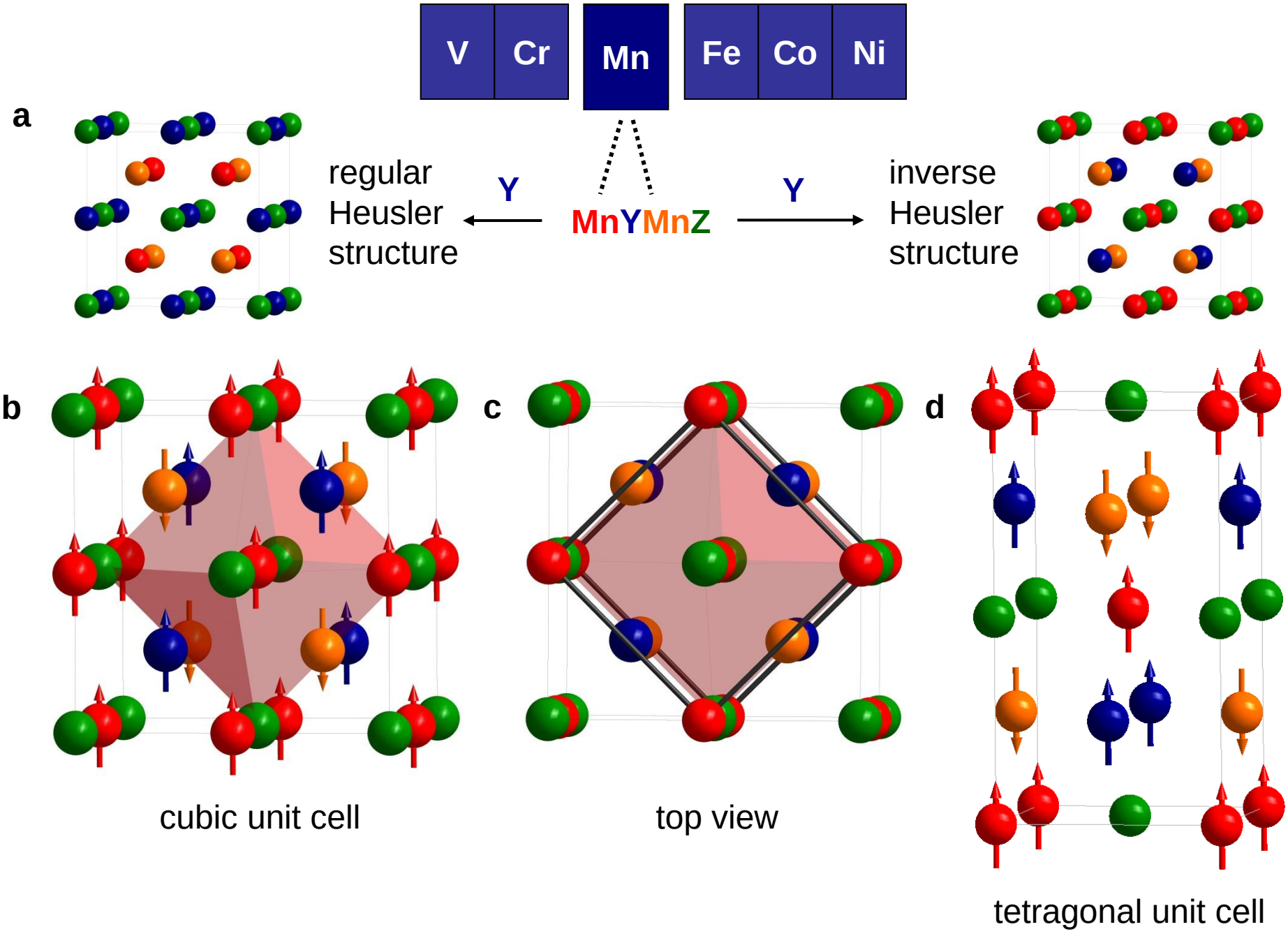
V
Cr
Mn
Fe
Co
Ni
a
regular
Heusler
structure
Y
MnYMnZ
Y
inverse
Heusler
structure
b
c
d
cubic unit cell
top view
tetragonal unit cell

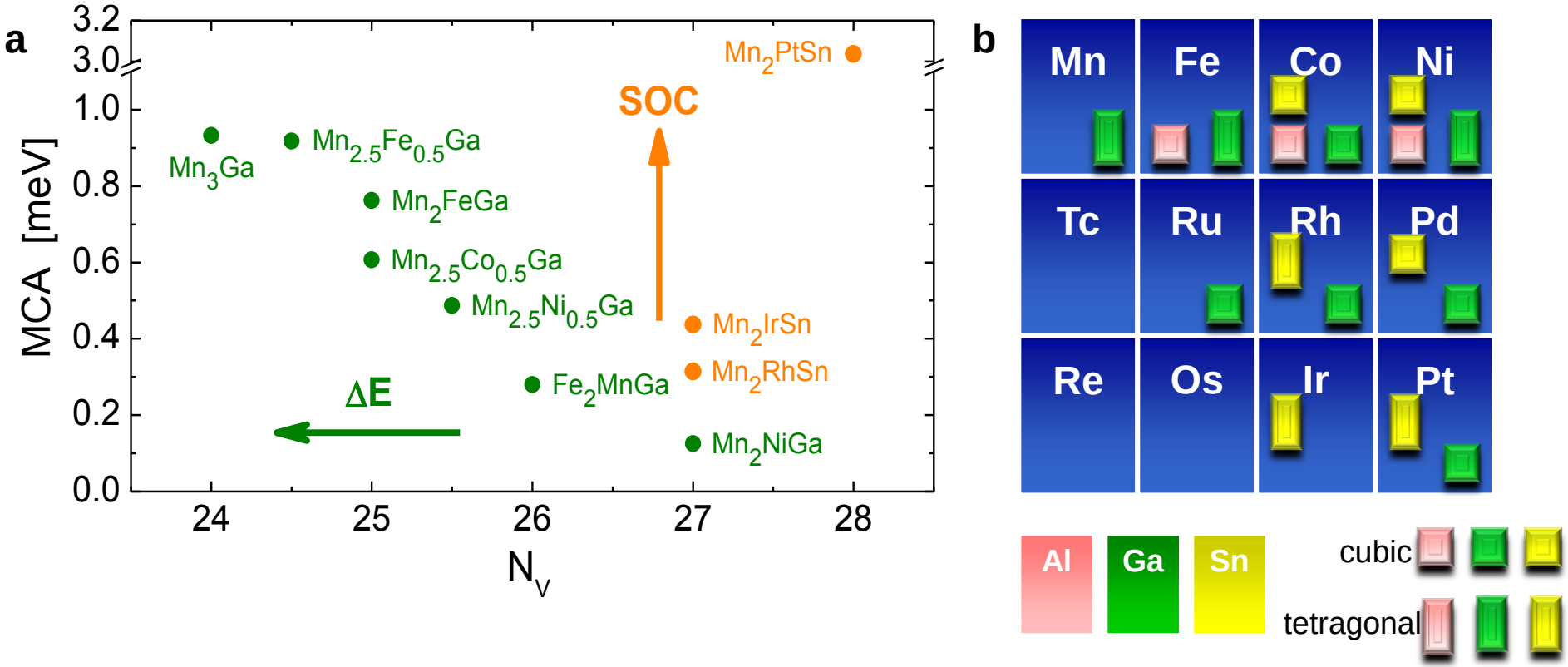
a
MCA [meV]
3.2
3.0
1.0
0.8
0.6
0.4
0.2
0.0
24
25
26
27
28
N_V
Mn2PtSn
SOC
Mn3Ga
Mn2.5Fe0.5Ga
Mn2FeGa
Mn2.5Co0.5Ga
Mn2.5Ni0.5Ga
Mn2IrSn
Mn2RhSn
ΔE
Fe2MnGa
Mn2NiGa
b
Mn
Fe
Co
Ni
Tc
Ru
Rh
Pd
Re
Os
Ir
Pt
Al
Ga
Sn
cubic
tetragonal

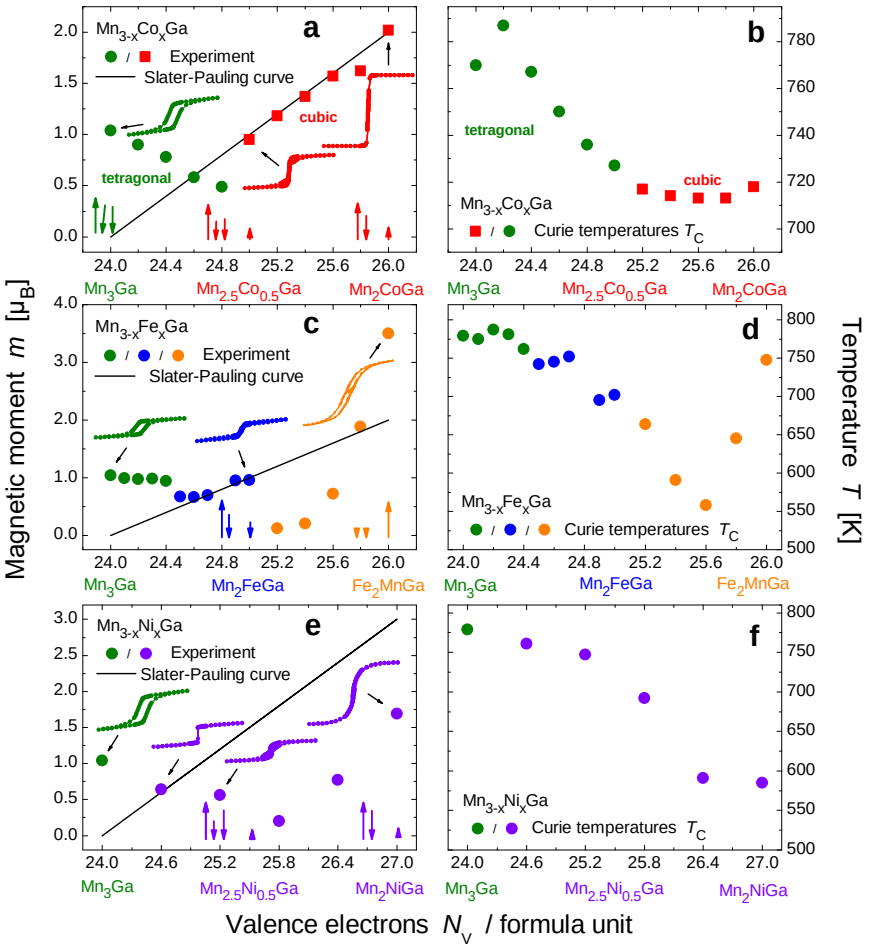
a
b
c
d
e
f
Mn3-xCoxGa
Mn3-xFexGa
Mn3-xNixGa
Experiment
Slater-Pauling curve
Curie temperatures TC
tetragonal
cubic
Mn3Ga
Mn2.5Co0.5Ga
Mn2CoGa
Mn2FeGa
Fe2MnGa
Mn2.5Ni0.5Ga
Mn2NiGa
Magnetic moment m [μB]
Temperature T [K]
Valence electrons NV / formula unit

Supplementary information:

Design scheme of new multifunctional Heusler compounds for spin transfer torque applications

J. Winterlik[1], S. Chadov[1], V. Alijani[1], T. Gasi[1], K. Filsinger[1], B. Balke[1], G. H. Fecher[1], C.A. Jenkins[1,2], J. Kübler[3], G. D. Liu[4], L. Gao[5], S. S. P. Parkin[5] & C. Felser[1*]

[1]*Institute of Inorganic and Analytical Chemistry, Johannes Gutenberg - University, 55099 Mainz, Germany*

[2]*Advanced Light Source, Lawrence Berkeley National Laboratory, Berkeley, CA, 94720, USA*

[3]*Institute of Solid State Physics, Technische Universität, 64289 Darmstadt, Germany*

[4]*School of Material Sciences and Engineering, Hebei University of Technology, Tianjin 300130, China*

[5]*IBM Research Division, Almaden Research Center, San Jose, CA 95120, USA*

To whom correspondence should be addressed; E-mail: felser@uni-mainz.de

Calculational details

All calculations were performed by means of the first-principle band-structure fully-relativistic version (A. Perlov, A. Yaresko, V. Antonov. Spin-polarized relativistic linear muffin-tin orbitals package for electronic structure calculations, PY-LMTO, unpublished) of the standard linearized muffin-tin orbitals approach. The exchange–correlation part of the effective potential was treated by using the Vosko–Wilk–Nusair parameterization[1] of the local-density approximation. The relative stability of the unit cell geometry was determined by calculating the total energy as a function of the *c/a* ratio at constant volume (see Supplementary Figure 1). The latter condition follows from both experimental and theoretical estimations that the changes of a volume are related with a significantly larger energy scale comparing to the changes of geometric form. The volume was thus determined only once by optimizing the cubic structure for each system. The magnetic anisotropy was calculated according to its definition, as the total energy difference between states with magnetization direction along the tetragonal strain (001) and in the perpendicular direction (010).

Synthesis and characterization of tetragonal Mn_2YZ Heusler compounds

Mn_2YZ bulk samples were prepared by repeated arc melting of stoichiometric amounts of high purity elements in argon atmosphere. To avoid oxygen contamination a Ti sponge was used as an oxygen absorber. The samples were melted three times and turned over in-between to guarantee for sufficient homogeneity. The resulting polycrystalline ingots were afterward annealed in evacuated quartz tubes for two weeks at temperatures in the range of 573 - 1273 K, depending on the respective composition of the alloys. Flat disks were cut from the ingots and polished for further investigations of the bulk samples.

For x-ray powder diffraction (XRD), a part of the sample was ground to a fine powder. The XRD measurements were carried out at room temperature using a Seifert XRD 3003 PTS diffractometer equipped with a Cu K_α x-ray tube. Rietveld refinements of the experimental data were carried out using the TOPAS ACADEMIC software package[2]. The magnetic properties were investigated using a superconducting quantum interference device (SQUID, Quantum Design MPMS-XL-5). Small, nearly spherical sample pieces of approximately 20 mg were used in these measurements. Supplementary Table 1 shows the determined structural and magnetic properties for certain tetragonal Heusler compounds and alloys.

The results of the Fe Moessbauer experiments are displayed in Supplementary Figure 3. The spectra were measured at room temperature in transmission mode.

References

1. Vosko, S. H., Wilk, L. & Nusair, M. Accurate spin-dependent electron liquid correlation energies for local spin density calculations: A critical analysis. *Can. J. Phys.* **58,** 1200–1211 (1980).

2. Coelho, A. TOPAS ACADEMIC, version 4.1 (2007).

Supplementary Figure 1: Determination of the relative phase stability. The total energy difference between cubic and tetragonally distorted phases calculated as a function of *c/a:* $\Delta E_{total} = E_{\text{total}}(c/a) - E_{\text{total}}(c/a = 1)$. The red and blue points mark the non-stable and stable configurations, respectively. **a**, The Mn_3Ga system. The insets show the corresponding spin-resolved band structures and densities of states for the cubic (c/a = 1) and distorted (c/a = 1.3) cases. The bold curves correspond to the spin channel, which exhibits the van

Hove singularity at the Fermi energy in the cubic case. The latter is obvious in the band structure (at R, X, Γ and M symmetric points in the Brillouin zone, symmetry group 119) and leads to a high peak of DOS at E_F in this spin channel. The tetragonal distortion lifts this degeneracy by moving the states away from the Fermi energy, which reduces the DOS peaks and stabilizes the system at *c/a*=1.3. **b.** The shape-memory alloy Mn_2NiGa. The system exhibits two stable states at *c/a*=1 and *c/a*=1.23, both characterized by the absence of the van Hove singularities leading to a dips of DOS at E_F. In the non-stable configuration (*c/a*=1.1) the singularity in R-X *k*-direction leads to a sharp DOS peak at E_F.

Supplementary Figure 2: Effect of the tetragonal strain on the orbital structure. The current example corresponds to the Mn_3Ga system. The horizontal bars mark the *d*-energy levels of the octahedrally- (Mn-I) and tetrahedrally-coordinated (Mn-II) atoms calculated at the Γ point of the Brillouin zone. Left or right orientation of a bar distinguishes the “up” or “down” spin channels, respectively (also indicated by black arrows). The size of a bar corresponds to the relative spectral weight of the certain symmetry distinguished by color. In the cubic crystal (*c/a*=1) the *d*-orbitals group in twofold e_g (z^2, x^2-y^2) and threefold t_{2g} (*xy*, *xz*, *yz*) representations of the octahedron symmetry group, marked by violet and light-green, respectively. By undergoing tetragonal strain along the *z*-axis (*c/a*=1.3), the out-of-plane orbitals split out from the in-plane ones. In particular, the e_g-orbitals at E_F, which carry the van Hove singularity in the “down” spin channel, split into x^2-y^2 (blue) and z^2 (violet) above and below the Fermi energy, thereby reducing the corresponding DOS peak.

Supplementary Figure 3: Moessbauer spectroscopy of Fe_2MnGa. The ^{57}Fe Moessbauer spectrum of Fe_2MnGa exhibits a very small hyperfine magnetic splitting of approximately 13 kOe on the Fe atoms. The corresponding magnetic moments of Fe atoms were deduced about 0.09 μB. This finding demonstrates that the total magnetic moment of Fe_2MnGa is almost completely determined by the Mn atoms.

Supplementary Table 1: Experimentally measured properties of tetragonal Mn_2-based Heusler compounds. N_V is the number of valence electrons per formula unit, m_S are the saturation magnetic moments, T_C the Curie temperatures, and H_c the coercivities.

Alloy	N_V	*c/a*	m_S	T_C	H_c
Mn_3Ga	24	1.28	1.04	779	453
Mn_2FeGa	25	1.43	0.96	702	56.9
$Mn_{2.7}Co_{0.3}Ga$	24.6	1.28	0.58	750	282
Mn_2Ga	17	1.30	1.41	723	102
Mn_2RhSn	27	1.09	1.87	305	55.2
Mn_2PtSn	28	0.95	3.69	374	78.8
Mn_2NiGa	25	1.21	1.69	585	32.6

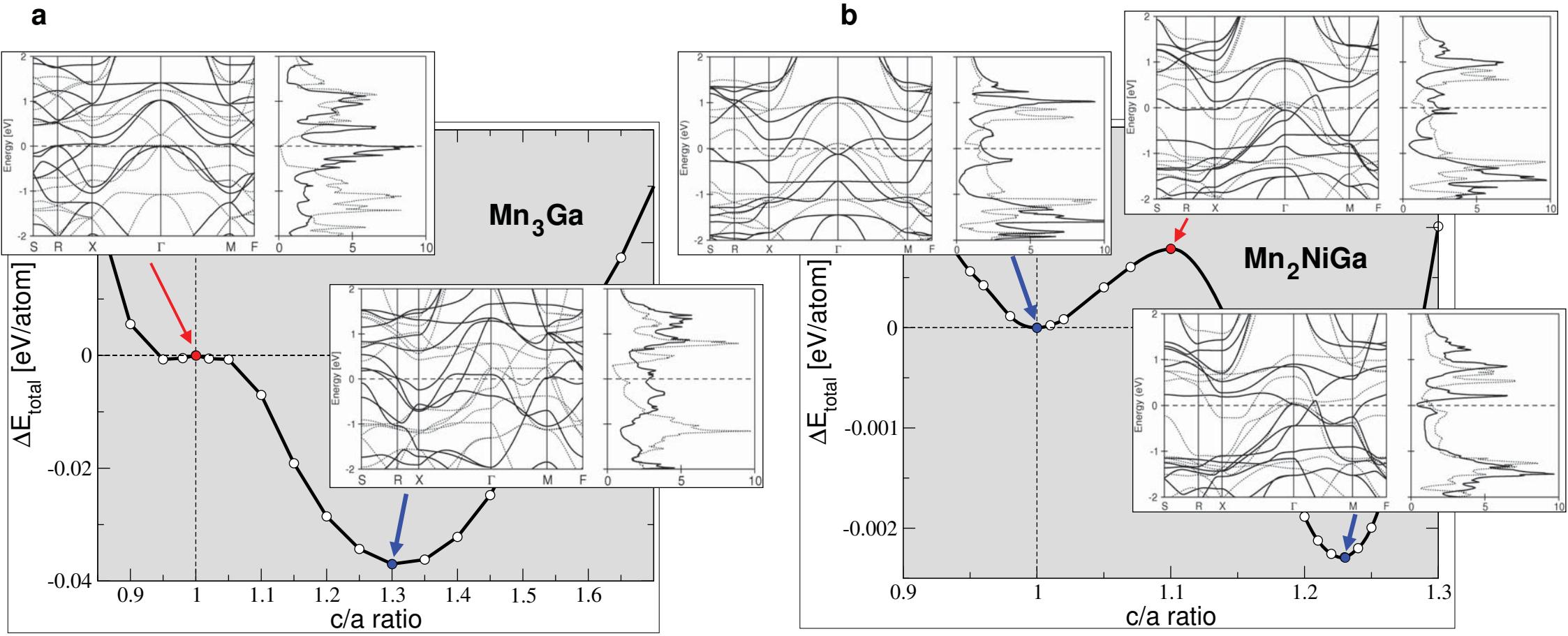
a
b
Mn3Ga
Mn2NiGa
ΔEtotal [eV/atom]
c/a ratio
Energy (eV)
S R X Γ M F

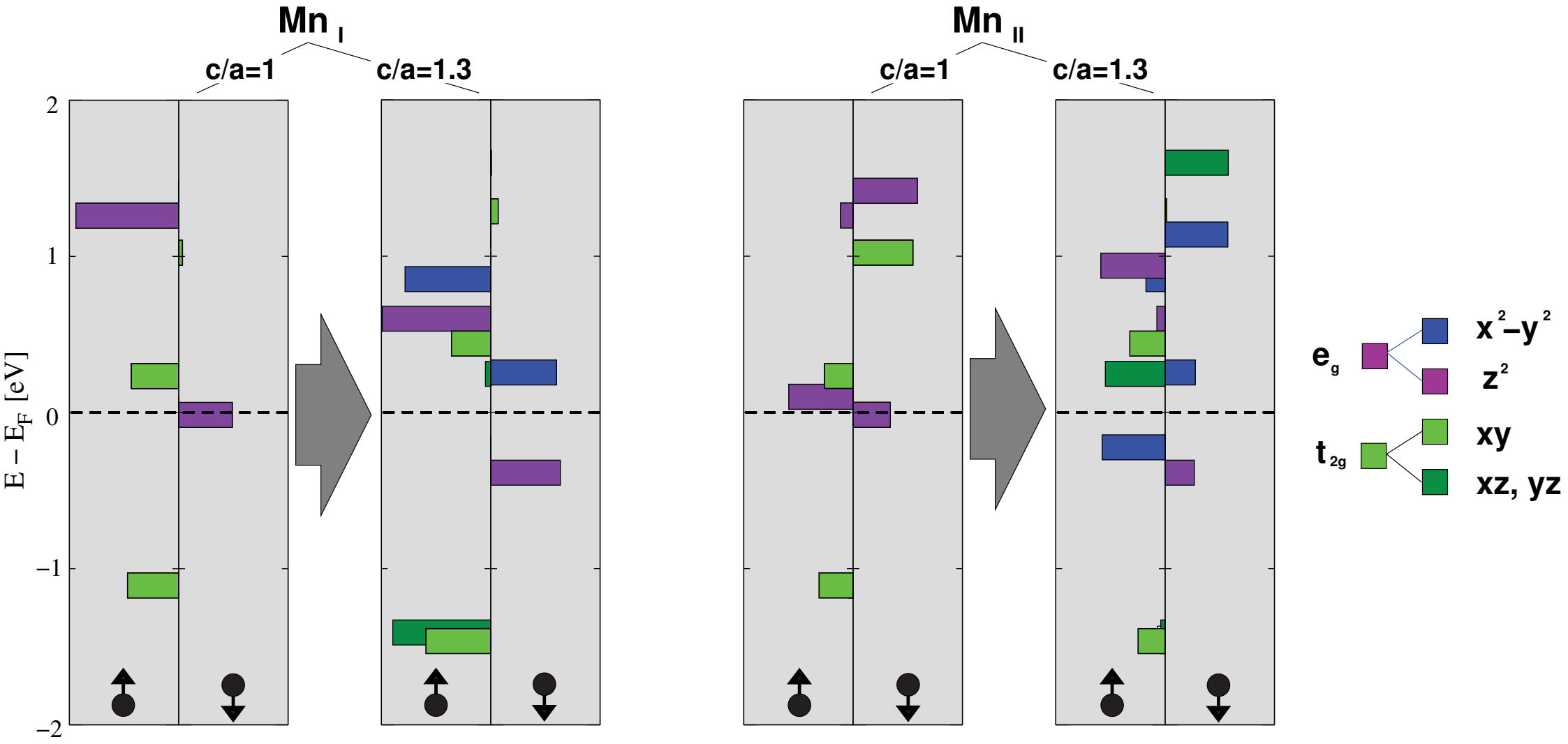
Mn I
c/a=1
c/a=1.3
Mn II
c/a=1
c/a=1.3
E – E_F [eV]
2
1
0
−1
−2
e_g
x²–y²
z²
t_2g
xy
xz, yz

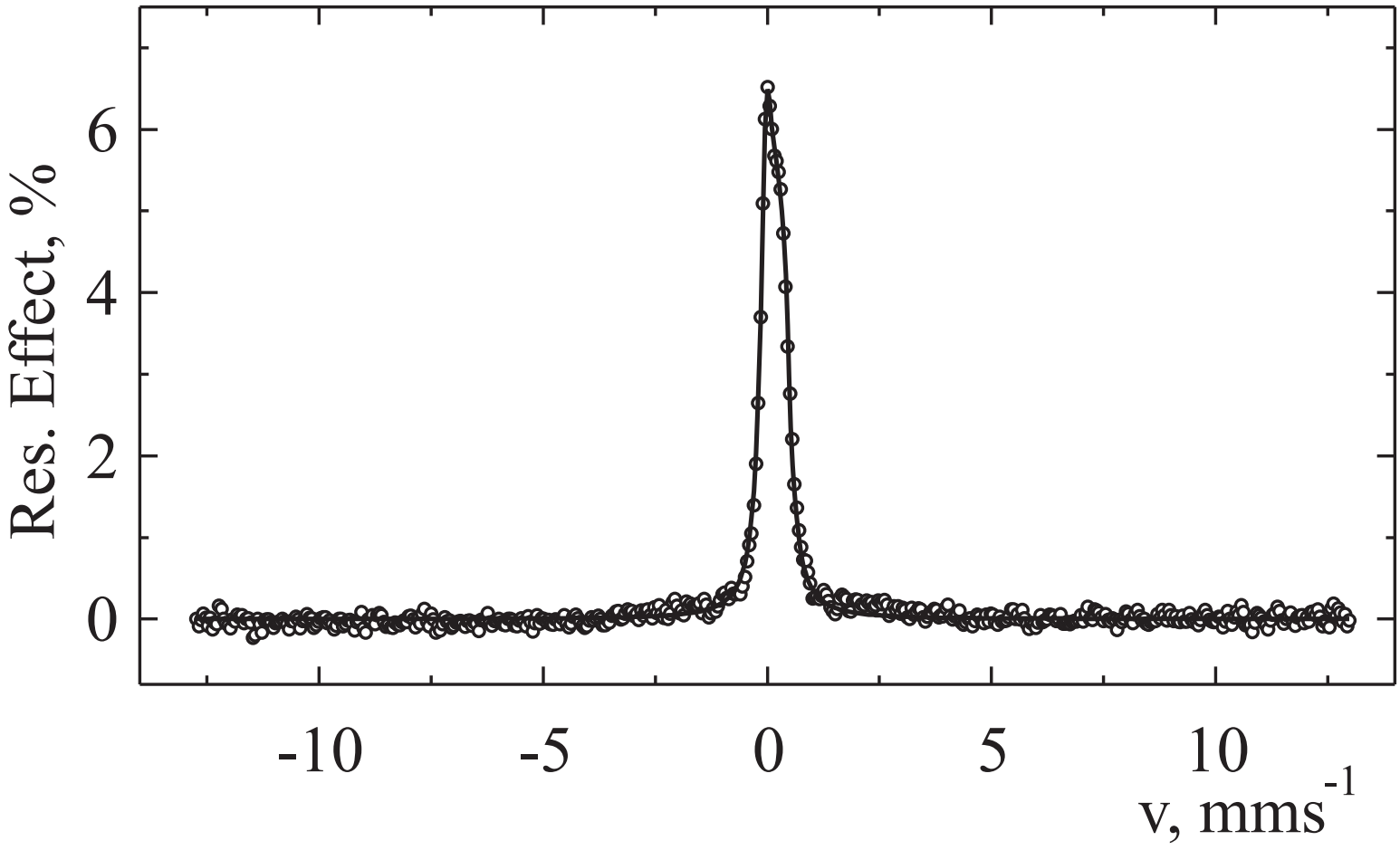
Res. Effect, %
6
4
2
0
-10
-5
0
5
10
v, mms-1